buildings

MDPI

Article

A Data-Mining-Based Novel Approach to Analyze the Impact of the Characteristics of Urban Ventilation Corridors on Cooling Effect

Xiaohan Shen [1], Hua Liu [2], Xinyu Yang [1], Xin Zhou [1,*], Jingjing An [3] and Da Yan [4]

[1] School of Architecture, Southeast University, Nanjing 210096, China; shen-xiaohan@seu.edu.cn (X.S.); 220220186@seu.edu.cn (X.Y.)
[2] Architecture and Engineering Co., Ltd. of Southeast University, Nanjing 210096, China; liuh@adriseu.com
[3] School of Environment and Energy Engineering, Beijing University of Civil Engineering and Architecture, Beijing 100084, China; anjingjing@bucea.edu.cn
[4] School of Architecture, Tsinghua University, Beijing 100084, China; yanda@tsinghua.edu.cn
* Correspondence: zhou-x06@seu.edu.cn

Abstract: The appropriate design of urban ventilation corridors (VCs) can improve the urban thermal environment, thereby reducing urban energy consumption and promoting sustainable urban development. However, existing research lacks a comprehensive grasp of the characteristics of VCs from multiple dimensions and quantitative analysis of its cooling effect. We propose a novel approach based on data mining to comprehensively consider the morphological and environmental characteristics of VCs and explore the correlation between VC characteristics and the cooling effect. Selecting Nanjing as an example, a comprehensive index system was constructed, the cooling effect of the VC was investigated, and the optimal range of VC index with different underlying surface types was obtained. Results revealed that the cooling effect is closely related to the underlying surface, leading to a temperature difference of up to 5.4 °C. The VC cooling range can vary from 13 to 600 m. The recommended optimal parameter intervals for different VCs were determined. Finally, targeted strategies to alleviate the heat island effect were proposed for different underlying surface types. The study output contributes to the design of VCs, which is of great significance in alleviating the urban heat island effect and promoting sustainable development of cities.

Keywords: urban environment; sustainability; ventilation corridor; cooling effect; urban heat island effect; data mining

check for updates

Citation: Shen, X.; Liu, H.; Yang, X.; Zhou, X.; An, J.; Yan, D. A Data-Mining-Based Novel Approach to Analyze the Impact of the Characteristics of Urban Ventilation Corridors on Cooling Effect. *Buildings* **2024**, *14*, 348. https://doi.org/10.3390/buildings14020348

Academic Editor: Emin Açıkkalp

Received: 12 December 2023
Revised: 11 January 2024
Accepted: 24 January 2024
Published: 26 January 2024

Copyright: © 2024 by the authors. Licensee MDPI, Basel, Switzerland. This article is an open access article distributed under the terms and conditions of the Creative Commons Attribution (CC BY) license (https://creativecommons.org/licenses/by/4.0/).

1. Introduction

1.1. Relationship between Urban Heat Island and Ventilation Corridors

In recent years, due to population growth and the disorderly expansion of cities, the urban heat island (UHI) effect has become more significant. The urban heat island effect refers to the phenomenon that the temperature in the city center is higher than that in the suburbs [1]. It is affected by factors such as energy consumption, expansion of impervious underlying surfaces like buildings and roads, and reduction of green spaces. Many studies have shown that UHIs can lead to slow vegetation growth, increased cooling energy consumption [2], deterioration of microclimate and outdoor thermal comfort [3], and adverse effects on biological health [4–6]. Therefore, to realize the sustainable development of the city, it is necessary to formulate strategies to alleviate UHI according to the characteristics of the city.

As an effective way to mitigate UHI, the urban ventilation corridor (VC) has attracted the attention of many researchers. Adequate urban ventilation can bring cool and fresh natural air from the suburbs to the city center, which can improve outdoor thermal comfort and disperse air pollutants [7]. The effectiveness of VCs has been demonstrated in many studies. Hea et al. [8] found that precinct ventilation cooling potential could significantly reduce urban heat island intensity (UHII), and every 0.1 increase in relative wind velocity

ratio corresponded to a 0.09–0.5 °C reduction in precinct UHII. Liu et al. [9] pointed out that the range of the reduction of VCs in mean UHI is between 0.3 and 1.33 °C. Another study [10,11] pointed out that the climate problems caused by urban expansion and industrial development can be solved by VCs that flow through areas with low temperatures, alleviate the UHI effect, and improve the livability of the city.

1.2. Factors Affecting the Cooling Effect of VCs

- Indexes of morphological characteristic

The cooling effect of VCs is affected by their morphological characteristics. To make full use of the cooling capacity of VCs, many scholars have studied the spatial form of VCs and put forward corresponding construction suggestions. Among them, the length, width, and wind direction of VCs are of concern to researchers as indicators that can be directly regulated in planning and design [12,13]. According to the urban climate characteristics of Stuttgart, Kress [14] proposed that the aspect ratio of the street should be between 2 and 4, the length of the corridor should be greater than 1000, and the width of the corridor should be greater than 30 m. Givoni [15] pointed out that an angle of 20–30 degrees between the dominant wind direction and the street direction in summer can promote airflow. Brown [16] proposed a minimum width of VCs of 100 m. Hea et al. [8] found that the precinct ventilation performance significantly varied with the precinct morphological characteristics, while the influence of street orientation was insignificant. Verein Deutscher Ingenieure (VDI) [17] defines VCs as an alignment, which should be as wide as possible (more than 50 m) and are better to be straight lines. Matzarakis [18] concluded that the factors that affect VCs include street rectilinear length, width, and height. Many cities in China have formulated the control range of the urban VC index at a block scale for the length [19], width [20], wind direction [21], street height–width ratio, and building density [22].

- Indexes of environmental characteristic

In addition to the morphological factors of the VC, the surrounding environment of VCs also plays an important role in improving the ventilation capacity and enhancing the cooling effect of VCs. In recent years, many studies have quantitatively analyzed the influence of the surrounding environment on VCs from two environmental characteristics: surface roughness [8] and underlying surface type [23].

As an indicator of urban morphological characteristics, surface roughness can effectively characterize the construction environment of VCs, which is one of the important environmental attributes of VCs [24]. Based on the aerodynamic concept, there are many representative variables that describe surface roughness, including surface roughness length, zero-plane displacement length, blending height [25], and frontal area index (FAI) [26], among others. One of the commonly used indicators is FAI. Several studies have pointed out that FAI positively correlates with surface temperature and negatively correlates with wind velocity ratio [27]. At a neighborhood scale, Hea et al. [8] revealed the cooling potential of precinct ventilation performance. They pointed out that the architectural form with low surface roughness can be selected to improve the local precinct ventilation performance to achieve a better thermal environment. From an urban-scale perspective, the ventilation effect and surface temperature are also affected by FAI. Liu [9] showed that FAI and roughness length affect ventilation capacity and also affect the cooling effect. The maximum reductions in multiyear mean UHII can reach 0.89 °C.

As an indicator of the environmental characteristics of VCs, the underlying surface type can effectively determine the environmental types and explore the characteristics of different types of VCs. On the urban scale, buildings, roads, green spaces, and water bodies have a great influence on the cooling effect of VCs [28]. Lai et al. [23] pointed out that daytime land surface temperature (LST) varied with the underlying surface in the VC. The LST of water is obviously lower than that of stone. Wu et al. [29] proved that urban green infrastructure at the urban scale has a significant impact on the cooling effect

of VCs. Shi et al. [30] divided VCs into different local climate zones (LCZ) and concluded that LCZB (scattered trees) had the best mitigation effect on UHII (−0.40 °C). Therefore, to obtain the optimal cooling effect, it is better to determine the layout of VCs according to the characteristics of the urban underlying surface [31].

1.3. Research Aims

In summary, most studies analyze the cooling effect of VCs from a single dimension of morphological or environmental characteristics and lack a comprehensive grasp of the characteristics of VCs from multiple dimensions. This leads to an incomplete understanding of the factors that affect VCs, which may lead to limitations in the analysis results and the inability to maximize the cooling effect of VCs in planning and construction. In addition, there is less quantitative analysis of the cooling effect of the VC. The implementation of urban VC construction needs to obtain quantitative data in line with local climate and morphological characteristics. Therefore, it is necessary to consider the morphological and environmental characteristics of VCs comprehensively and explore the quantitative relationship between these factors and the cooling effect of VCs. The research output will contribute to the rational construction of VCs, which are of great significance in alleviating the UHI effect and promoting the sustainable development of cities.

An index system was constructed in this study to achieve the above goals, which can describe both the morphological and environmental characteristics of VCs. Taking Nanjing as an example, a novel approach based on data mining was proposed to explore the correlation between VC indexes and LST. At the same time, based on the cooling effect, the optimal range of the VC index with different underlying surface types was investigated. The quantitative relationship between VC indexes and the surface temperature was explored, and the cooling effect of the VC was analyzed. Finally, from the perspective of VC design, this study proposed targeted strategies to alleviate the heat island effect and improve the urban thermal environment according to the distribution characteristics of VC indexes under different underlying surface types.

The remainder of this article is organized as follows. The methodology, including VC-recognition technology, calculation of ventilation corridor indexes, correlation analysis, and k-means clustering, is presented in Section 2. The results and analysis are presented in Section 3, followed by the discussion and conclusion in Sections 4 and 5, respectively.

2. Methodology

2.1. Overall Technical Approach

The overall technical approach of this study is shown in Figure 1. This study starts with constructing a geographic information system (GIS) database. The FAI of the study area is calculated using the digital elevation model (DEM), building data, and meteorological data. Based on the FAI map, VCs are identified using the least cost path (LCP) method. After obtaining the VCs, their index system is established, including length, angle, surface roughness, cooling width, LST, and underlying surface type. Based on these indexes, data analysis is divided into two steps: correlation analysis and k-means cluster analysis. Key VC indexes that have an impact on the cooling effect under different underlying surfaces are extracted using correlation analysis. Furthermore, VC indexes are selected as clustering variables, and the VCs are classified using the k-means clustering algorithm to identify the type of VC with the best cooling effect under different underlying surfaces.

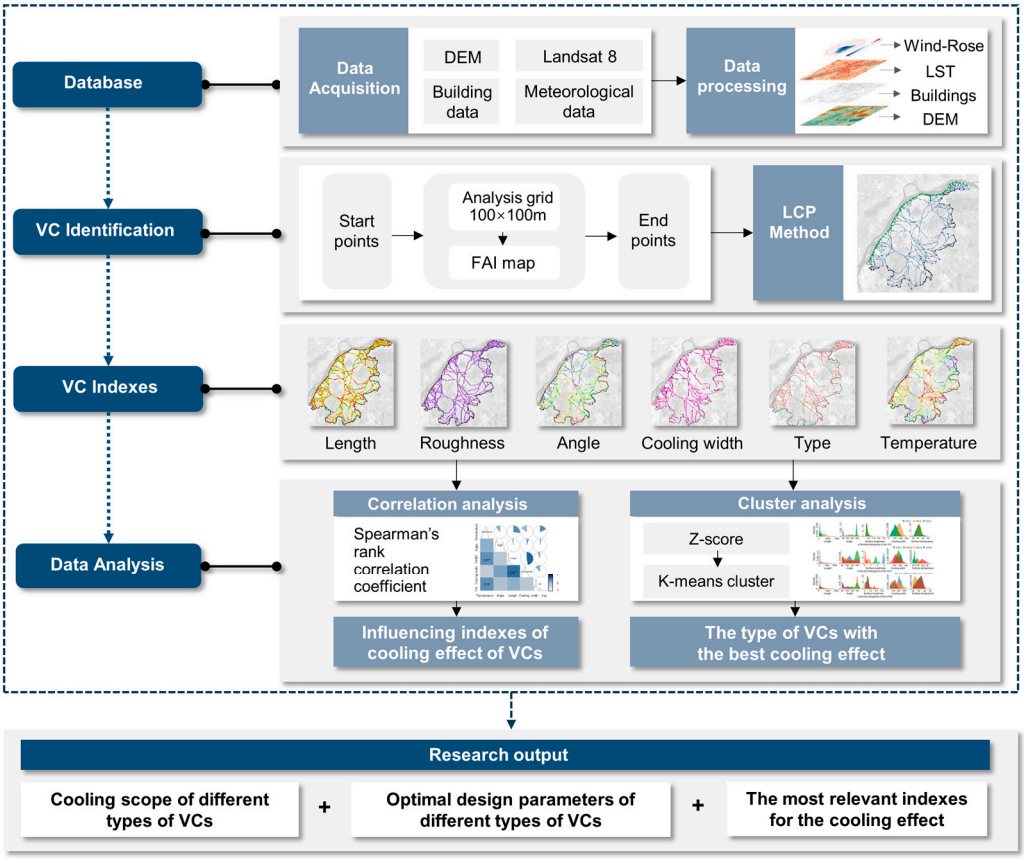


Figure 1. Technical approach of this study.

2.2. Data Source

Considering the urban development level, representativeness of the ventilation corridors, and typicality of the climate, the central urban area of Nanjing, with 2066 km^2 in total, was selected as the research area (118°73′ E–119°29′ E, 31°62′ N–32°24′ N). The research area is shown in Figure 2 by the red dotted box; it includes the districts of Xuanwu, Gulou, Jianye, Qinhuai, Yuhuatai, Qixia, and Jiangning. Since the 21st century, Nanjing has experienced a period of rapid urban expansion. The area of the built-up region increased by 796 km^2 between 2000 and 2012 [32]. Due to the rapid urban expansion in the study area, the UHI effect is significant [33]. This leads to a general increase in summer temperature in the region and a significant increase in heat stress and heat exposure [34]. The climate in Nanjing is characterized by a typical subtropical monsoon. It is hot and humid in summer, and the highest temperature can reach 41 °C in recent years. Therefore, it is of great significance to improve Nanjing's thermal environment by optimizing the design of VCs. The surface types of the study area of Nanjing are rich, with the water area accounting for 11.4% of the total area of the city, and the forest coverage rate of the city is 31%. As urban cold sources, the water and vegetation not only reduce the ambient temperature but also have an important impact on the formation of VCs.

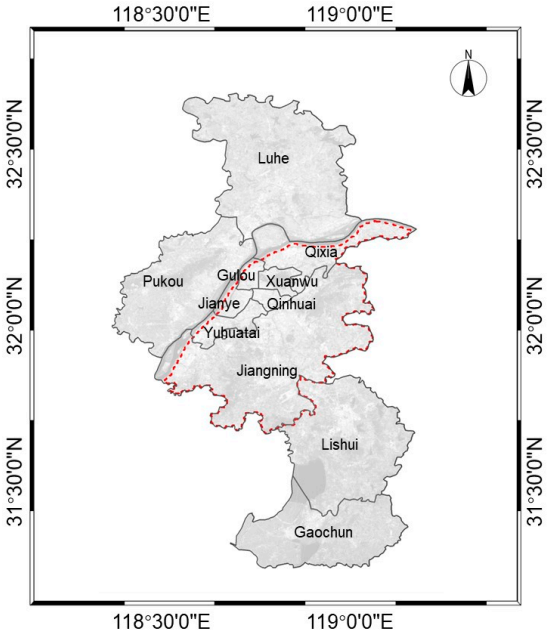


Figure 2. Location of study area.

The data used in this study included DEM, building data, LST, and meteorological data (Table 1). ASTER GDEM with a resolution of 30 m was used as the DEM. Building data, including building height, number of building layers, and land area, were obtained from the Baidu map. Landsat 8, with a thermal infrared band resolution of 30 m, was used to calculate LST and underlying surface types. The following three factors were mainly considered in the selection of Landsat 8 satellite data: (1) Since the building data is from 2022 and the meteorological data is from 1984 to 2018, the LST data should be selected between 2018 and 2022. However, due to the new coronavirus epidemic, the rate of urban expansion has slowed down. There was little change in building data between 2019 and 2022. Therefore, data should be selected as close as possible to 2018. (2) Because the focus of this study is the cooling effect of VCs in summer, the months are limited to June, July, and August. (3) Considering the accuracy of the data, the cloud cover should be less than 10%. Based on these three criteria, the Landsat 8 data on 28 August 2019, with a cloud amount of 2.12%, was finally selected as the basic data. The Landsat 8 data contained 11 bands: Band 10 (the thermal infrared band) was used for LST, Bands 3 and 6 were used for water extraction, and Bands 3 and 4 were used for vegetation extraction. The frequency of different wind directions in summer in Nanjing was obtained from meteorological data, and the wind direction in summer was mainly concentrated in the range of 90–202.5°.

Table 1. Data sources and descriptions.

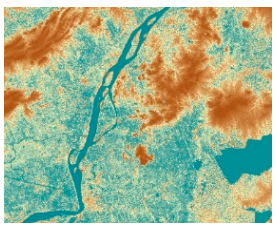
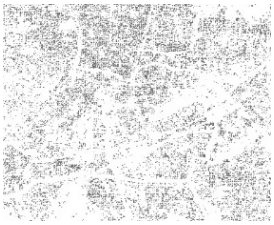
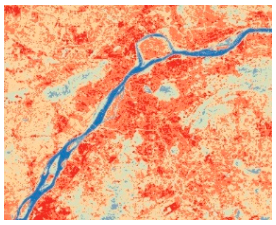
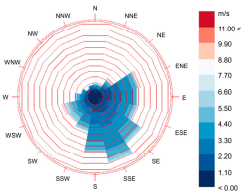
Data	Descriptions	Source	Sample
Digital elevation model	Elevation of terrain	ASTER GDEM (30 m) Geospatial Data Cloud, gscloud.cn (accessed on 20 November 2022)	

Table 1. *Cont.*

Data	Descriptions	Source	Sample
Building data	Building outline, height, floor, and types, 2022	Baidumap, map.baidu.com (accessed on 20 November 2022)	
Land surface temperature	Band 1–11 28 August 2019	Landsat 8 OLI_TIRS (30 m) Geospatial Data Cloud, gscloud.cn (accessed on 20 November 2022)	
Meteorological Data	Frequency of different wind directions, 1984–2018	CSWD dataset for Nanjing	

2.3. Identifying the Ventilation Corridors

The identification of VCs was divided into the following four steps:

Step 1. Determine the starting point and endpoint of VCs

According to the Nanjing meteorological data, the dominant wind direction in Nanjing in summer is the SE-NW direction. Therefore, the starting points of VCs were set on the southeast side of the research boundary, and the endpoints of VCs were set on the northwest side of the research boundary. The length of the southeast side of the boundary was 94 km, and that of the northwest side was 174 km. According to the length of the boundary, sixty starting points were set on the southeast boundary with an interval of 2.9 km, and forty ending points were set on the northwest boundary with an interval of 2.35 km.

Step 2. Determining the size of the analysis grid

After determining the starting and endpoints, this study divided the research area into grids. There are two commonly used grids: uniform grids and irregular grids. Irregular grids can avoid cutting large buildings and are conducive to maintaining the integrity of the building. However, it leads to the neglect of space forms except the building, such as open spaces, water, and mountains. In contrast, although uniform grids segment large buildings, they are more conducive to the identification and analysis of different spatial types. Therefore, uniform grids are more suitable for the study of VCs. In addition, existing studies have proven that 100 m resolution can effectively support urban climate research [35], and most urban-scale studies have applied 100 × 100 m grids [36–38]. Therefore, 100 × 100 m uniform grids were adopted as the analysis grid of this study.

Step 3. Calculate FAI

As Equations (1) and (2) and Figure 3 show, FAI is the ratio of the total projection area of the building under a specific wind direction (θ) to the area of the analysis grid of the wind direction, which is one of the most important indicators of surface roughness [26].

The value range of FAI is mostly within [0, 1]. The larger the FAI, the greater the barrier effect of the building against the wind.

$$\lambda_{f(\theta)} = \frac{A_F}{A_T} = \frac{nb_{f(\theta)}h_{f(\theta)}}{A_T} \quad (1)$$

$$\mathrm{FAI} = \sum_{\theta=1}^{N} \lambda_{f(\theta)} B_\theta \quad (2)$$

where A_F is the total area of each building or hill face projected onto the plane normal to the incoming wind direction (m^2), A_T is the plane area of the study site (m^2), $\lambda_{f(\theta)}$ is the FAI at a particular wind direction, N represents wind directions, and B_θ is the annual wind frequency at a particular wind direction.

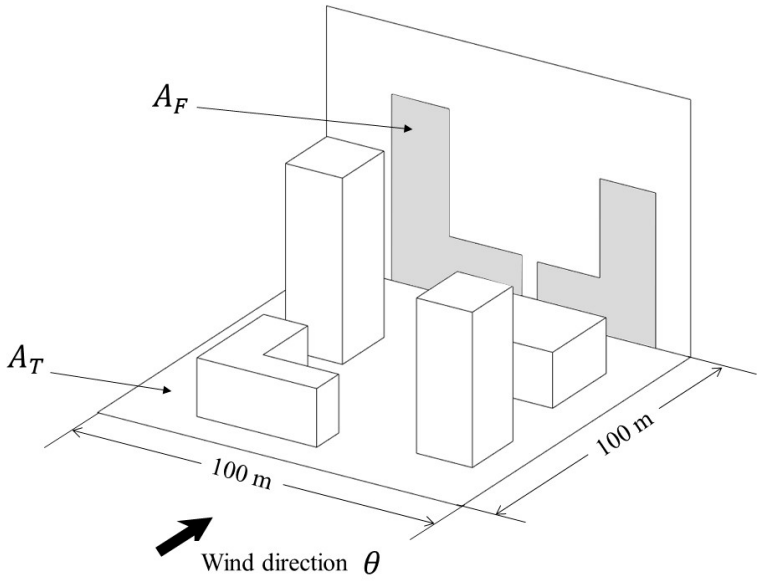


Figure 3. Diagram of the FAI calculation method.

Step 4. Calculating the ventilation path based on the least cost path method

The LCP method is simple and fast and is suitable for large-scale and complex spatial types [39]. The basic principle of the minimum cost path is to find the path connecting the starting point and the endpoint based on the FAI map calculated by Step 3 so that the total cost on the path is minimized [40]. The effectiveness of the LCP method in identifying the ventilation path has been proven by previous studies through actual measurements or CFD simulations [36,38,41]. Therefore, it is widely used in urban-scale VC identification. In this study, the LCP method was used to identify the path with the lowest airflow cost on the FAI map. This method takes FAI as the cost value, calculates the path with the minimum cost from the starting point to the endpoint, and then represents the corridor position with an intuitive graph. In this study, there were 60 starting points and 40 ending points, and 2400 LCPs were generated according to the FAI map.

This study further subdivided the LCP path according to the following process to generate VCs, as shown in Figure 4. First, according to wind direction, the LCP path was broken into N short paths in a single wind direction. Then, continuous short paths with $\theta_i < 5^\circ$ were connected. Finally, the M VCs for analysis were obtained. Figure 4 shows the relationship between LCP paths, short paths, and VCs.

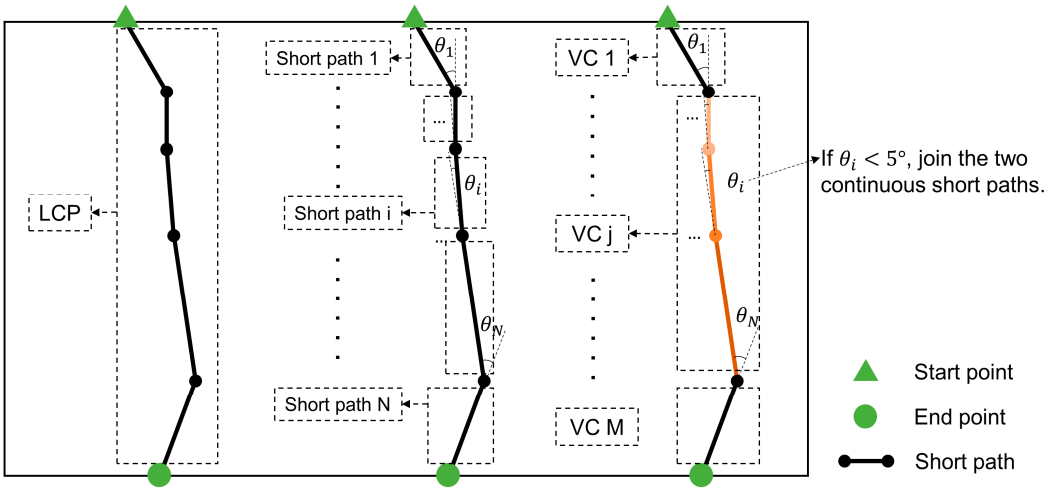


Figure 4. The relationship between LCP paths, short paths, and VCs.

2.4. VC Indexes

Based on existing studies, the underlying surface type, length, angle, surface roughness, cooling width, and surface temperature of VCs were selected as the key indicators to describe the characteristics of VCs quantitatively.

The definition and calculation of the VC index are as follows:

(1) Underlying surface type

The study area was divided into three types based on the underlying surface's characteristics: water, vegetation, and impermeable surface. In this study, Landsat 8 data were used to classify the underlying surface types. The Landsat 8 data contained 11 bands; the combination of different bands can accurately identify the boundaries of vegetation and water bodies [42]. The three types of underlying surfaces were classified as follows:

(a) Water

The modified normalized difference water index (MNDWI) method can identify the water bodies within the study area [43]. If MNDVI > 0, the area is water. Therefore, this study used Equation (3) to calculate MNDWI:

$$\text{MNDWI} = \frac{\text{Band 3} - \text{Band 6}}{\text{Band 3} + \text{Band 6}} \tag{3}$$

where Bands 3 and 6 are the green and mid-infrared bands in the Landsat 8 data, respectively.

(b) Vegetation

Normalized difference vegetation index (NDVI) is an important index that evaluates vegetation coverage. The calculation Formula (4) is as follows:

$$\text{NDVI} = \frac{\text{Band 4} - \text{Band 3}}{\text{Band 4} + \text{Band 3}} \tag{4}$$

where Bands 4 and 3 are the near-infrared and visible red bands, respectively.

(c) Impervious surface

After accounting for areas under vegetation and water, the remaining areas were defined as impervious surface areas.

The underlying surface type of the VC was determined according to the area where the VC was located. Where multiple underlying surface types existed in one VC, the VC was cut off at the junction of different underlying surfaces. Therefore, based on the underlying surface identification results, all VCs were subdivided to ensure that there was only a single type of underlying surface in each VC. Finally, the VCs were divided into

impervious surface ventilation corridor (VCI), vegetation ventilation corridor (VCV), and water ventilation corridor (VCW).

(2) Length

The length of the VC was the total length of each short path contained in the VC and was calculated using Equation (5):

$$\mathrm{L} = \sum_{i=1}^{n} L_i \tag{5}$$

where L_i is the length of the i-th short path, and n is the number of short paths in the VC.

(3) Angle

The angle of the VC was the average angle of each short path contained in the VC and was calculated as in Equation (6):

$$\mathrm{A} = \sum_{i=1}^{n} \frac{A_i L_i}{L} \tag{6}$$

where A_i is the angle of the i-th short path.

(4) Surface roughness

The surface roughness of the short paths was calculated. By stacking the short paths on the FAI map, the average of the FAI values of all grids that the short path passed through was calculated, and this value was the surface roughness of the short paths. The surface roughness of the VC was the average surface roughness of all short paths contained in the VC and was calculated as shown in Equation (7):

$$\lambda = \sum_{i=1}^{n} \frac{\lambda_i L_i}{L} \tag{7}$$

where λ_i is the FAI of the i-th short path.

(5) Cooling width

Figure 5 shows the determination of the average cooling width of short paths. First, the temperature breakpoints within 600 m on both sides of the short path are identified. Second, the nearest temperature breakpoints were selected on both sides of the short path, and the distance between the pair of temperature breakpoints was calculated. Finally, the average value of the distance between the pairs of temperature breakpoints was used as the cooling width of the short path, calculated as shown in Equation (8):

$$\mathrm{D} = \sum_{j=1}^{n} \frac{d_j}{n} \tag{8}$$

where D is the cooling width of the short path; d_j is the distance between the j-th pair of temperature break points.

The second step was to calculate the cooling width of the VC. The average cooling width of each short path contained in the VC was considered the cooling width of the VC and was calculated as shown in Equation (9):

$$\mathrm{W} = \sum_{i=1}^{n} \frac{D_i L_i}{L} \tag{9}$$

where D_i is the cooling width of the i-th short path.

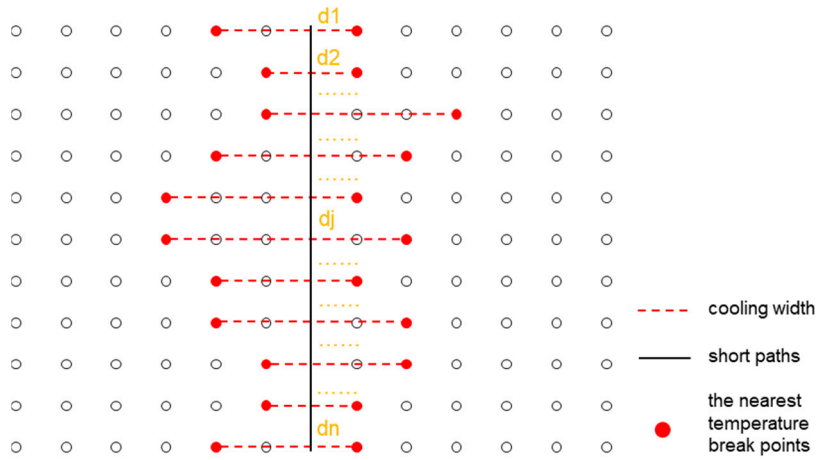


Figure 5. The method of determining the cooling width of the short path.

(6) LST

First, the Landsat-8 dataset was preprocessed, including radiometric calibration, image cropping, and atmospheric correction. Then, the mono-window algorithm was used to calculate the LST [44]. This algorithm is simple and feasible and has a high precision. The calculation is shown in Equations (10)–(14):

$$T_S = \frac{1}{C}\{a(1-C-D)+[b(1-C-D)+C+D]\times T_b - D\times T_a\} \quad (10)$$

$$T_b = \frac{K_2}{\ln\left(\frac{K_1}{L_\lambda}+1\right).} \quad (11)$$

$$L_\lambda = \frac{DN\times(L_{max}-L_{min})}{255}+L_{min} \quad (12)$$

$$C = \varepsilon\tau \quad (13)$$

$$D = (1-\varepsilon)[1+\tau(1-\varepsilon)] \quad (14)$$

where T_S is the real surface temperature (K), a and b are regression coefficients, T_b is the pixel brightness temperature of the thermal infrared band (K), K_1 and K_2 are the preset constants of the pre-launch satellite obtained from the Landsat8 TIRS image metadata file, T_a is the average atmospheric temperature (K), C and D are intermediate variables, L_{max} and L_{min} are maximum and minimum thermal radiation fluxes ($W\cdot m^{-2}\cdot sr^{-1}\cdot \mu m^{-1}$), ε is the surface emissivity, and τ is the transmittance of the atmosphere in the thermal infrared band.

Based on the results of LST, the temperatures of short paths were calculated. The short paths on the LST map were overlaid, and the average LST values of all the grids that the short paths passed through were calculated and taken as the LST of the short paths. The average LST of the short paths contained in the VC was taken as the LST of the VC and was calculated as shown in Equation (15):

$$T = \sum_{i=1}^{n}\frac{T_i L_i}{L} \quad (15)$$

where T_i is the LST (°C) of the i-th short path.

2.5. Correlation Analysis

The data distribution of this study does not conform to the normal distribution; there are outliers, and the sample size is relatively large. Therefore, Spearman's rank correlation coefficient (calculated using Equation (16)) was used to evaluate the correlation between each index and LST. The value range of Spearman's rank correlation coefficient falls within $[-1, 1]$; close to 1 is a positive correlation, and close to -1 is a negative correlation.

$$\mathrm{r} = 1 - \frac{6\sum_{i=1}^{n} D_i^2}{n(n^2-1)} \tag{16}$$

where r is the Spearman's rank correlation coefficient, D_i is the difference in ranks of the "i-th" element, n is the number of data points in the samples.

2.6. Cluster Analysis

The units of different variables selected in this paper are different, and the data range gap is large. In order to avoid the scale difference of variables affecting the accuracy of the algorithm, the Z-score method is used to normalize and ensure that different variables are on a similar scale. The calculation formula is shown in Equation (17):

$$x_z = \frac{x - \overline{x}}{x_\sigma} \tag{17}$$

where x_z is the normalized variable value, x is the original value of the variable, $\overline{x}$ is the average value of the variable, x_σ is the standard deviation of the variable.

The k-means clustering algorithm has a good processing effect on large-scale data sets and is suitable for high-dimensional data. The clustering results can intuitively present the characteristics of each type and are easy to understand. Therefore, based on the research objectives, data characteristics, and algorithm advantages, the k-means clustering algorithm was chosen. The goal of clustering is to minimize the distance of each point to the cluster center in each category. The principle of the k-means clustering algorithm is as follows: First, k objects are randomly selected as the initial clustering centers. Then, the Euclidean distance from each sample to the center is calculated. According to the Euclidean distance, the new cluster center is generated. When iterated continuously, the result converges when the cluster center no longer changes, ending the clustering [45]. The Euclidean distance is calculated as shown in Equation (18):

$$Distance(O_i, O_j) = \sqrt{\sum_{k=1}^{n} \left(O_{ik} - O_{jk}\right)^2} \tag{18}$$

where O_{ik} and O_{jk} are the k-dimensional coordinates of points O_i and O_j, respectively, and n is the number of clustering variables.

In addition, the elbow method is used to determine the number of cluster centers using the relationship between the SSE and K value. The relationship between the SSE value and k value is an 'elbow-shaped' line chart, and the corresponding k value of the elbow is the optimal clustering number of the cluster. The calculation of SSE is shown in Equation (19):

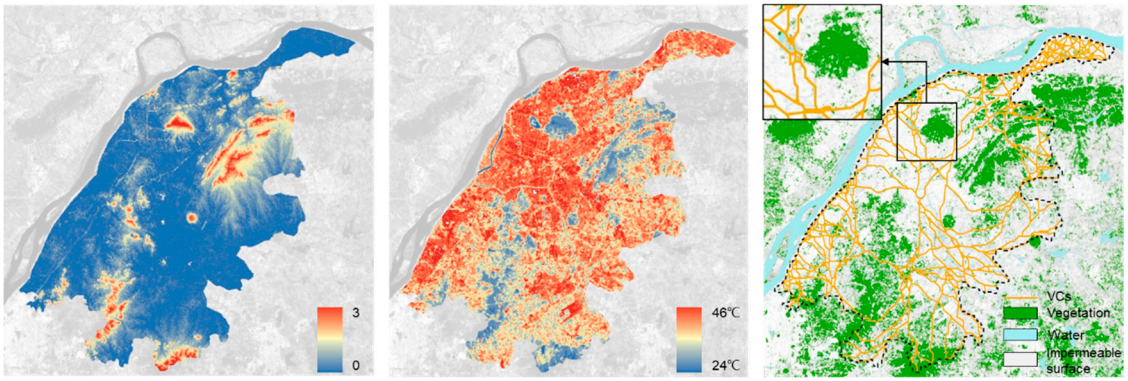
$$SSE = \sum_{i=1}^{K} \sum_{p \in L_i} \|p - q_i\|^2, \tag{19}$$

where p is the data object in the i-th class group L_i, q_i is the average value of all data objects in a class group, and k is the number of cluster centers.

3. Results and Analysis

3.1. The Overall Situation of the Research Area

The distribution of FAI is shown in Figure 6a. The average FAI of the entire study area, the impervious surface, water, and vegetation were 0.38, 0.27, 0.19, and 0.81, respectively. FAI represents the surface roughness: the larger the value, the rougher the surface. Due to the large number of mountains in the vegetation area, the FAI of vegetation was 0.54 higher than the average FAI of the impermeable surface. The water area is generally open, so FAI was the lowest.



(a) The distribution of FAI (b) the distribution of surface temperature (c) the distribution of VCs

Figure 6. The overall situation of the research area.

The distribution of surface temperature is shown in Figure 6b. The surface temperature of the study area was different from the FAI distribution. The overall trend of FAI was vegetation > impervious surface > water, while the overall trend of surface temperature was impervious surface > water > vegetation. The average temperature of the vegetation was 30.98 °C, that of the water body was 31.04 °C, and the overall average temperature of the study area was 34.76 °C. Therefore, it can be concluded that as a typical cold island, the surface temperature of the mountain and the water was significantly lower than that of the built-up area. The temperature differences reached 0.06–3.78 °C.

The VC paths identified using the LCP method are shown in Figure 6c. These paths show the ventilation situation of the study area and the typical characteristics of the spatial distribution of VCs. By comparing the types of underlying surfaces of the VCs, it can be found that VCs in the central area of Nanjing city bypassed the mountain and were mainly distributed along the river. In the built-up area, they were mainly distributed along roads, green spaces, and squares.

3.2. Distribution Characteristics of VC Indexes

The spatial distribution of the VC indexes is shown in Figure 7. The distribution of the VC lengths had no apparent regularity. The VCs around the vegetation were mostly parallel to the contours of the vegetation area and had lower temperatures. The VC with large surface roughness was mainly located near the vegetation. From the perspective of the cooling effect, the cooling width of the VC near the Yangtze River and the mountain was relatively large. At the same time, because the analysis was about the urban area, most of the underlying surface types of VCs were impervious surfaces.

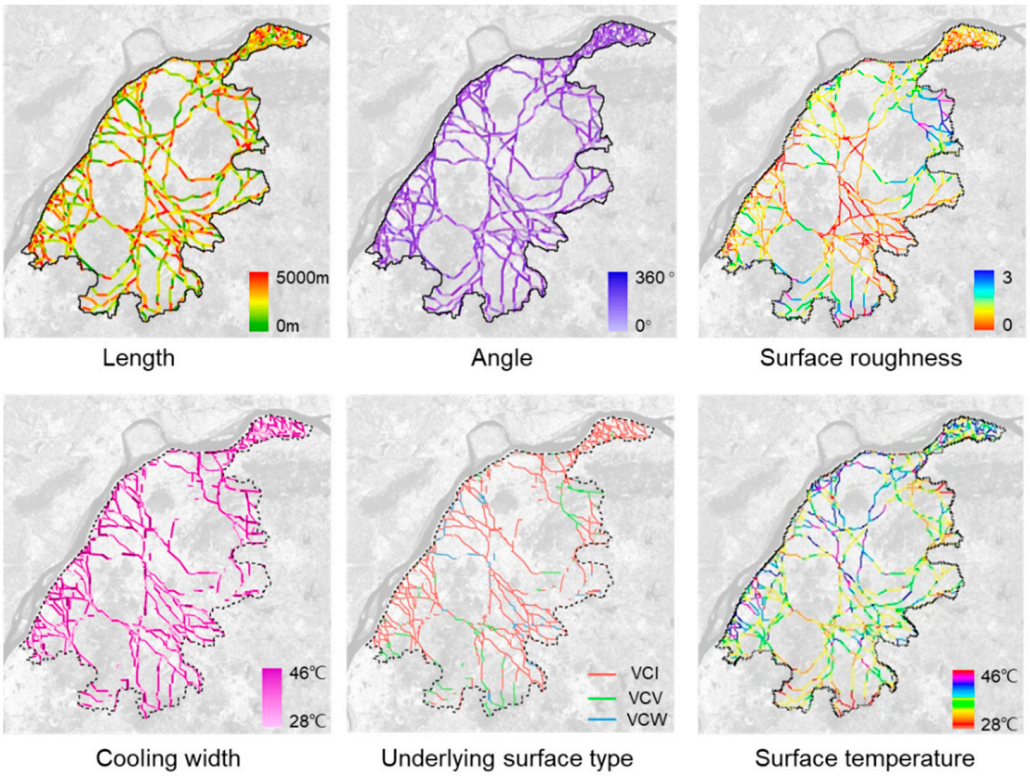


Figure 7. The spatial distribution of the VC indexes.

The distribution of the VC indexes for all kinds of VCs is shown in Figure 8a. The average length for the VCs in the Nanjing central area was 695 m, of which 51.5% were within 500 m, and 79.6% of VCs were within 1000 m. The angles were concentrated in the 90–202.5° range, accounting for 77%. As for the surface roughness, the average FAI of VCs was 0.193, and 78.1% of the FAIs of the VCs were within 0.2. The average cooling width of the VCs was 137 m, of which the cooling width of more than 200 m accounted for 12%. The distribution of VC types in Nanjing was extremely uneven. The number of VCIs was the largest, accounting for 75%. Also, 14.6% of the VCs were VCVs, and the VCW was the least, accounting for 10.4%. As for the LST, the temperature of VCs was mainly concentrated in the range of 30–40 °C, accounting for 91.2%, and the average value was 34.95 °C.

There were similarities and differences between the indexes of the three types of VCs with different underlying surfaces. The lengths of the three types of VCs were all concentrated within 1000 m, and the order of the average length was VCI (706 m) > VCV (608 m) > VCW (520 m). The distribution of the angles of different VC types, which were all concentrated at 90°, 135°, and 180°, was highly similar. Similar to the overall roughness distribution in the study area, the overall trend of the FAI of the VCs was VCV (0.4) > VCI (0.16) > VCW (0.13). The mean values of the width of the VCVs (148 m) and the VCWs (144 m) were larger than that of the VCIs (134 m). The width of the VCs was mostly within the range of 200 m. The proportion of the width of the VCWs greater than 200 m was the most, accounting for 22.3%. For the average temperature of the VC, VCI > VCV > VCW. The temperature differences reached 1.84–5.4 °C, with average values of 36, 32.44, and 30.6 °C for the VCI, VCV, and VCW respectively.

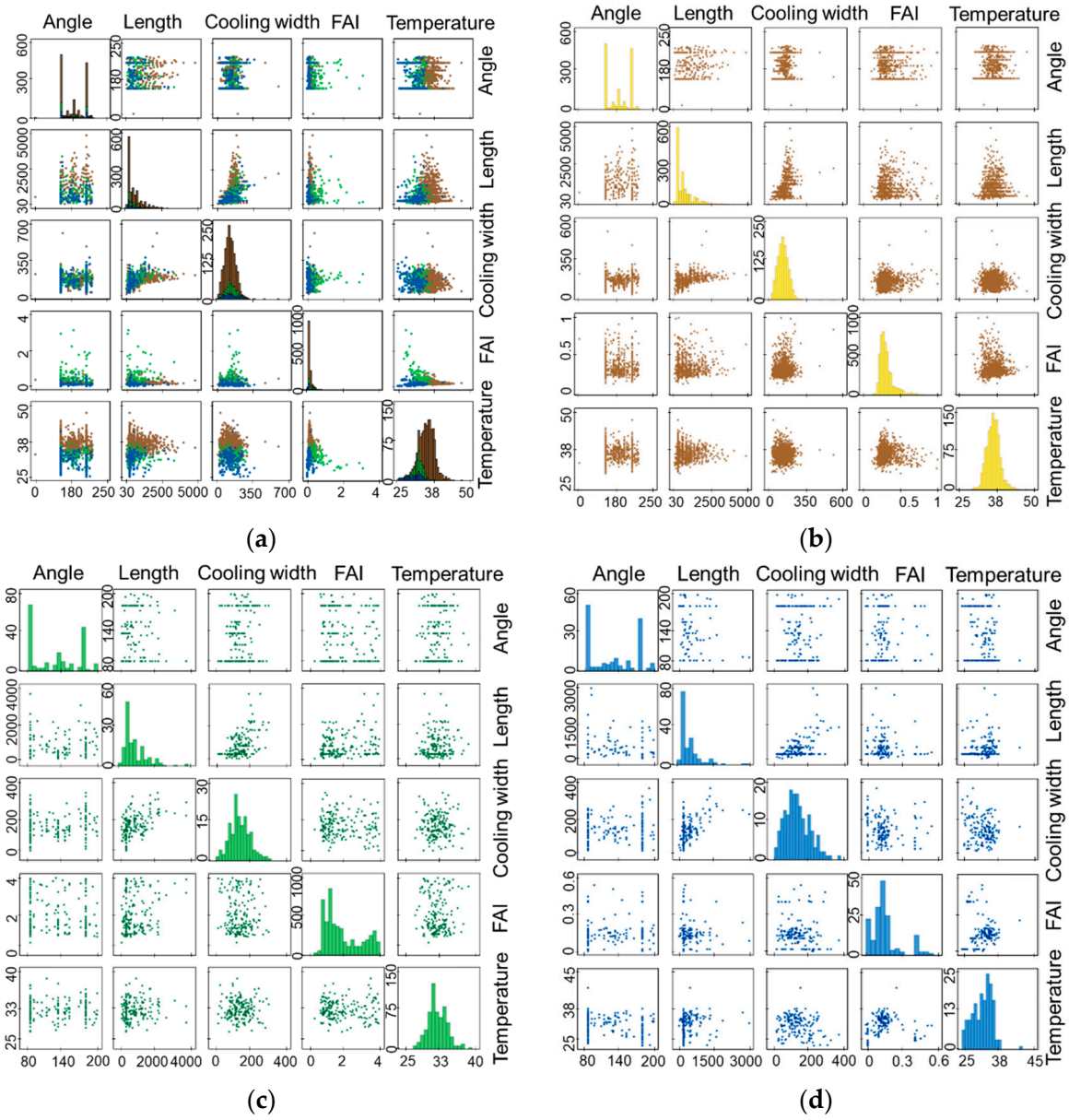


Figure 8. The index distribution of the VCs. (**a**) VC (VCI is the brown part, VCV is the green part, and VCW is the blue part). (**b**) VCI. (**c**) VCV. (**d**) VCW.

3.3. Influencing Factors of Cooling Effect of VCs

The correlation results of the VCs with different underlying surface types are shown in Figure 9. For VCI, there is a statistical relationship between the LST and length, but the degree of correlation is weak. At the same time, the width, angle, and roughness of the VCI have little effect on the LST. In addition, the calculation results of the cooling width of VCI are also the smallest, and its cooling effect on the land surface is not significant. For VCI, its ventilation effect in the city is stronger than the cooling effect. Due to the high temperature in the built-up area, the long VCIs accumulated heat; thus, they showed a poor cooling effect [46]. Therefore, in the construction of the VCI, the open space, such as water and vegetation, should be divided to supplement the cooling effect.

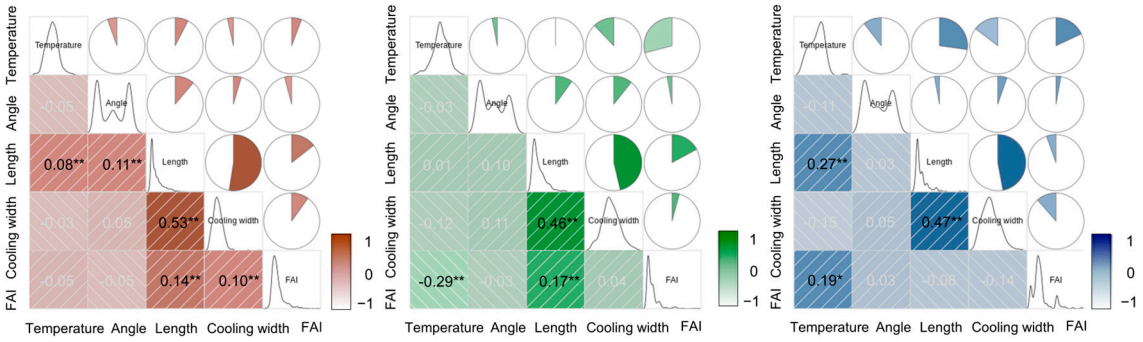


Figure 9. Correlation analysis results. (**a**) VCI. (**b**) VCV. (**c**) VCW. **: Correlation is significant at the 0.01 level (2-tailed); *: Correlation is significant at the 0.05 level (2-tailed).

As for the VCV, the temperature and roughness were significantly negatively correlated, as Figure 9b shows—the larger the roughness of the vegetation ventilation corridor, the lower the temperature of the VCV, and the better the cooling effect. When the roughness increased from 0.06 to 3.14, the temperature decreased from 37 to 27 °C. Mountainous areas had high roughness in the vegetation corridor, whereas open spaces within the city, such as large areas of grassland or shrubs, had low roughness, mostly [47,48]. Due to factors such as vegetation types, vegetation density, and altitude, the surface temperature of the mountains was significantly different from that of the urban constructed area [49]. Wang et al. also found the cooling effect of the mountain to have a certain relationship with vegetation type and density [28]. Most of the trees with lush leaves have strong transpiration and better cooling effect [50]. In contrast, the transpiration of shrubs, grasslands, etc., is slightly weaker, which results in a lower cooling effect. Similarly, the amount of vegetation planted is also critical. Therefore, trees and shrubs can be planted on existing grasslands to strengthen the cooling effect of vegetation corridors as much as possible without affecting the existing corridors.

For the VCW, Figure 9c shows a significant positive correlation between temperature, length, and roughness. The temperature of the VCW increases with the increase in the length and surface roughness, and the cooling effect decreases. When the length increased from 89 to 2991 m, the roughness increased from 0 to 0.65, and the VC temperature increased from 25 to 41 °C. The roughness of the water corridor was closely related to the construction intensity around the water—the more open the space near the water body, the lower the roughness of the VCW from the index. It can be seen that the lower the temperature of the VCW, the better the cooling effect. Therefore, when planning and designing VCWs, the openness around the water can be appropriately increased using measures such as the construction of parks around the water to enhance the cooling effect.

3.4. Typical VC Extraction and Feature Analysis

In this study, the VCIs were divided into VCI-1, VCI-2, and VCI-3 categories, mainly based on the angle and length. The detailed information on the index of each sub-category of the VCI is shown in Table 2 and Figure 10a. Comparing the average temperatures of sub-category VCIs, VCI-3 had the best cooling effect. The distribution of the temperature was relatively concentrated; thus, the temperature difference between the three sub-categories of VCIs was relatively small. The average temperature of VCI-2 was the highest (36.23 °C), while the temperature of VCI-3 was the lowest (35.87 °C), which is 0.2–0.4 °C lower than the other two categories. The angle of VCI-3 was mainly concentrated at about 175°. The length change ranged from 34 to 1200 m, and the average length was 455 m. The average length of VCI-2 was 1681 m; VCI-2 was much longer than VCI-3. By comparing the distribution characteristics of the three types of VCIs, the cooling effect was better when the VCI angle was approximately 175°, and the overall length was less than 1200 m. Therefore, the cooling

effect of VCIs can be improved by changing the angle and reducing the length. In VC planning, specific measures for urban construction-intensive areas include changing the direction of the VC and setting up local open spaces such as water bodies and vegetation to control the length of the VC.

Table 2. Clustering results of the VCI.

Category	Index	Minimum	Maximum	Mean
VCI-1	Angle (°)	90	135	102
	Length (m)	55	1354	439
	Cooling width (m)	29	300	119
	Surface roughness	0.05	0.82	0.16
	LST (°C)	29.30	44.67	36.08
VCI-2	Angle (°)	90	202	143
	Length (m)	271	4874	1681
	Cooling width (m)	119	310	191
	Surface roughness	0.09	0.72	0.17
	LST (°C)	31.46	42.03	36.23
VCI-3	Angle (°)	139	198	176
	Length (m)	34	1117	455
	Cooling width (m)	13	240	115
	Surface roughness	0.06	0.56	0.15
	LST (°C)	29.82	47.44	35.87

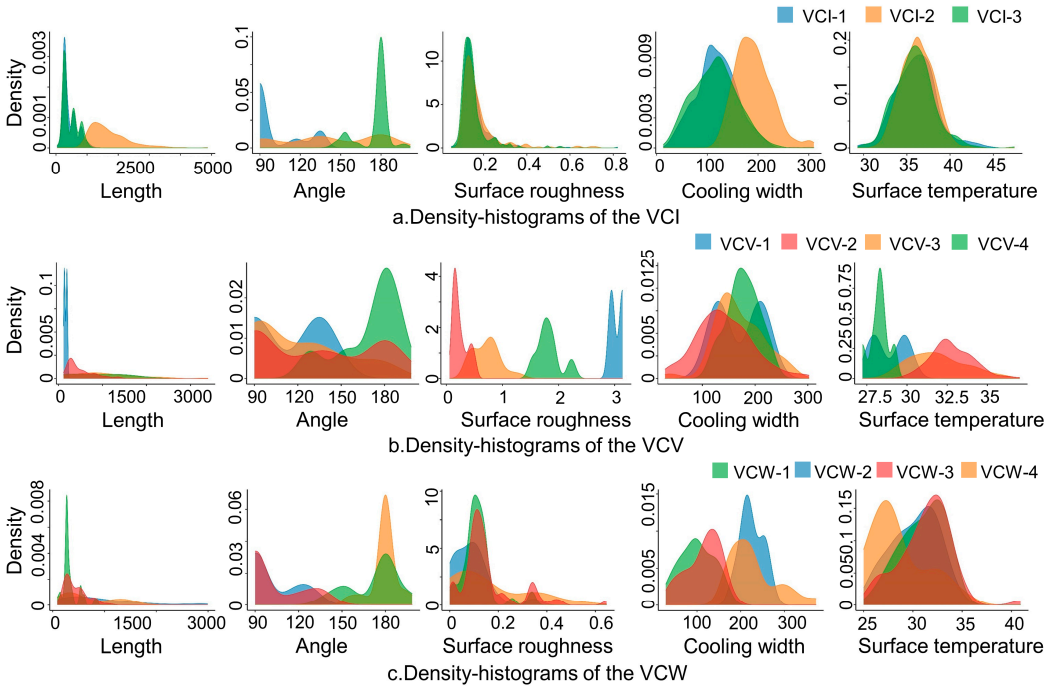


Figure 10. The density histograms of the clustering result.

The VCV can be divided into four categories (VCV-1, VCV-2, VCV-3, VCV-4) mainly based on the roughness of the VCV, as shown in Table 3 and Figure 10b. Comparing the average temperatures of various types of VCVs, the temperature of VCV-1 and VCV-4 was below 29 °C, which is 3–4.5 °C lower than that of the other two types. Therefore, these two types of corridors have a noticeable cooling effect. The most noticeable attribute feature of these two types of VCVs is that they have high roughness values, all of which were above 1.5 and up to 3.1, which is consistent with the correlation results in Section 3.2. Therefore, when designing VCVs, it is necessary to focus on retaining and broadening VCVs with

high roughness, that is, VCVs located around the mountain, and enhance the cooling effect of the area.

Table 3. Clustering results of the VCV.

Category	Index	Minimum	Maximum	Mean
VCV-1	Angle (°)	90	135	113
	Length (m)	135	191	163
	Cooling width (m)	130	210	170
	Surface roughness	2.94	3.14	3.04
	LST (°C)	27.94	29.84	28.89
VCV-2	Angle (°)	90	198	134
	Length (m)	115	1381	489
	Cooling width (m)	29	302	141
	Surface roughness	0.06	0.54	0.24
	LST(°C)	29.81	37.01	32.79
VCV-3	Angle (°)	90	180	120
	Length (m)	135	3396	1075
	Cooling width (m)	39	270	170
	Surface roughness	0.35	1.34	0.71
	LST (°C)	29.15	35.84	31.90
VCV-4	Angle (°)	129	191	170
	Length (m)	135	1765	850
	Cooling width (m)	128	223	199
	Surface roughness	1.54	2.23	1.82
	LST (°C)	27.23	29.21	28.26

VCW can be divided into four categories (VCW-1, VCW-2, VCW-3, VCW-4) mainly based on the angle and width of the VCW, as shown in Table 4 and Figure 10c. Comparing the average temperatures of various types of VCWs, the temperature of VCW-4 was 28.53 °C, which was 1.6–2.7 °C lower than that of the other three types. Therefore, VCW-4 had the best overall cooling effect, and the attribute range of this type of VCW was taken as the recommended construction range. When planning the construction of VCWs in Nanjing, the VCW angle can be concentrated at approximately 180°, and the VCW width should be as large as possible; most of them were above 200 m.

Table 4. Clustering results of the VCW.

Category	Index	Minimum	Maximum	Mean
VCW-1	Angle (°)	135	198	173
	Length (m)	89	856	335
	Cooling width (m)	28	167	99
	Surface roughness	0.01	0.34	0.12
	LST (°C)	25.95	34.51	31.02
VCW-2	Angle (°)	90	132	102
	Length (m)	251	2991	925
	Cooling width (m)	180	273	225
	Surface roughness	0	0.34	0.09
	LST (°C)	25.90	34.13	30.17
VCW-3	Angle (°)	90	146	104
	Length (m)	135 m	1105	441
	Cooling width (m)	30	187	115
	Surface roughness	0.01	0.65	0.15
	LST (°C)	25.62	40.92	31.27

Table 4. *Cont.*

Category	Index	Minimum	Maximum	Mean
VCW-4	Angle (°)	153	198	179
	Length (m)	271	1625	681
	Cooling width (m)	168	372	229
	Surface roughness	0	0.54	0.16
	LST (°C)	25.00	35.19	28.53

4. Discussion

4.1. The Influence of VCs on LST

From the above results, it can be seen that the LST of the VCs with different underlying surface types is also significantly different. The LST of the VCWs (30.6 °C) was lower than that of the VCVs (32.44 °C), and the LST of the VCIs (36 °C) was the highest. The temperature differences reached 1.84–5.4 °C. The wind corridor through the water and green space has a significant improvement effect on the LST. Previous studies yielded analogous conclusions. Shi et al. [30] pointed out that water bodies had the lowest average UHII, which indicates that it is more effective in mitigating UHI. Guo et al. [51] pointed out the effects of underlying surface types on the LST and verified them in four different cities. Therefore, to achieve the goal of urban sustainability, it is necessary to focus on protecting existing VCWs and VCVs. At the same time, the construction of VCWs and VCVs should be increased as much as possible. Because the cooling effect of the VCI is the weakest, VCWs and VCVs can be added to improve the thermal environment in the area where the LST is high, and only VCI passes [46,52,53].

4.2. Strategies for Enhancing the Cooling Effect of VCs

The above data analysis illustrates the relationship between the VC indexes and the LST. Operable strategies have been proposed to enhance the cooling effect of the VC. When designing urban VCIs, on the premise of ensuring the overall connectivity of the VCIs, the length of the VCIs can be reduced by setting up local VCWs or VCVs, and the length can be limited to within 1200 m to improve the overall cooling effect of VCIs. Similar results were observed in prior investigations. Fang et al. [54] found that VCs with impervious surface + vegetation + water have the lowest temperature and the largest ventilation benefit. Therefore, when the VCI is too long and cannot be interrupted, VCWs or VCVs parallel to the original VC can be added. By broadening the width of the VCs and the superposition of various VCs, the cooling potential of VCs can be comprehensively improved. In addition, the VCIs with an angle of approximately 175° have the best cooling effect in Nanjing. The angle of VCIs usually coincides with the direction of the urban road network [55]; therefore, their angle can be maintained at about 175° by adjusting the direction of the road.

For the development and utilization of VCVs, it is necessary to focus on the protection of existing VCVs, especially through the mountain parts, which have important cooling potential. In areas with harsh thermal environments, the cooling effect of VCVs can also be improved by local supplementary planting of trees to increase vegetation density [56]. Lan et al. [57] pointed out that the extensive greenery of VCs can enhance the overall cooling effect and have a synergistic mitigation effect. Wang et al. [58] found that trees exhibit a superior cooling effect compared to shrubs, with a temperature reduction of approximately 1.35 °C. Huang et al. [47] pointed out that there is a significant negative correlation between the forest canopy density and the surface temperature. The average LST of the study area decreased from 32.65 to 30.33 °C when the forest canopy density increased from 0.31 to 0.40.

For the VCW, the most important thing is to maintain the openness around the water to reduce the roughness of the VCW. The width of the VCWs significantly affects the cooling effect; it can be kept above 200 m by building hydrophilic squares and greenways. In addition, the direction of the linear water body can best be controlled at about 180°.

4.3. Limitations and Prospects

This study selected Nanjing in summer as an example and presented an approach to quantify VC characteristics and cooling effects. Construction strategies based on the cooling effect were proposed for different types of VCs. For the specific impact of the implementation of these strategies on the urban heat island effect, we consider quantitative research through numerical simulation in subsequent studies. The method proposed in this study is applicable across different seasons, years, and cities. In a follow-up study, we will also explore the changes in the cooling effect of VCs in the time and space dimensions. In the time dimension, the cooling effect of VCs during the day and night can be compared, and the influence of VCs on the urban thermal environment in different seasons will be explored. In the spatial dimension, the effect of VCs on different local climate zones can be compared.

The calculation of the FAI currently only considers the influence of elevation and buildings, ignoring the roughness of the vegetation. Vegetation has a certain influence on the accuracy of VC identification in the built-up area [47]. The types of vegetation in the built-up area are rich, and the spatial distribution is complex. It is difficult to quantify vegetation at the urban scale, which leads to the difficulty of vegetation modeling. In small and medium-scale studies, the method of LiDAR can be combined to assist in the modeling of vegetation [59]. Therefore, the consideration of vegetation roughness can be added to the calculation of FAI. This field can be further explored in the future.

5. Conclusions

Clarifying the quantitative relationship between the characteristics of urban VCs and the cooling effect will greatly improve the operability and controllability of VC construction. It is of great significance in alleviating the UHI effect and fostering the sustainable development of cities. Taking Nanjing as an example, a comprehensive index system was established in this study to describe the morphological and environmental characteristics of VCs. Through the Spearman rank correlation coefficient and k-means clustering, the accurate construction focus and optimal construction scope of the VC are obtained. The main conclusions are as follows:

The cooling effect and cooling width are closely related to the underlying surface. The difference in underlying surface types can lead to a temperature difference of up to 5.4 °C between VCs. Similarly, the proportion of the cooling width of VCWs greater than 200 m is the most, accounting for 22.3%. The cooling effect of the VCVs and VCWs is significantly better than that of the VCIs.

Through correlation analysis, this study found that length and surface roughness are the focus of VC construction. The significant correlation indexes of the VCV and VCW were roughness and length and roughness, respectively.

The optimal range of the VC index with different underlying surface types was obtained based on the cooling effect, and the corresponding construction strategy was proposed. The angle of the VCIs can be maintained at about 175° by adjusting the direction of the road, and the length can be reduced by setting up local VCWs or VCVs. For the VCV, the cooling effect is strong when the roughness is between 1.5 and 3.1. Therefore, the VCV through the mountainous area is the focus of protection. For the development and utilization of VCWs, the most important thing is to maintain the openness around the water to reduce the roughness and increase the cooling width.

Author Contributions: Methodology, X.Z. and J.A.; validation, D.Y.; software, D.Y.; formal analysis, X.Y.; investigation, J.A.; resources, J.A.; data curation, J.A. and D.Y.; writing—original draft preparation, X.Z., X.S., X.Y. and H.L.; writing—review and editing, X.Z., X.S. and H.L.; visualization, X.S. and X.Y.; supervision, D.Y.; project administration, H.L.; funding acquisition, X.Z. and J.A. All authors have read and agreed to the published version of the manuscript.

Funding: This work was supported by the National Science Foundation (52078117), National Science Foundation (52108068), and "Zhishan" Scholars Programs of Southeast University (2242021R41145).

Data Availability Statement: Data are available upon request due to privacy.

Conflicts of Interest: Author Hua Liu was employed by the company Architecture and Engineering Co., Ltd. of Southeast University. The remaining authors declare that the research was conducted in the absence of any commercial or financial relationships that could be construed as a potential conflict of interest.

References

1. Oke, T.R. The energetic basis of the urban heat island. *Q. J. R. Meteorol. Soc.* **1982**, *108*, 1–24. [CrossRef]
2. Gan, V.J.L.; Wang, B.; Chan, C.M.; Weerasuriya, A.U.; Cheng, J.C.P. Physics-based, data-driven approach for predicting natural ventilation of residential high-rise buildings. *Build. Simul.* **2022**, *15*, 129–148. [CrossRef]
3. Tong, Z.; Luo, Y.; Zhou, J. Mapping the urban natural ventilation potential by hydrological simulation. *Build. Simul.* **2021**, *14*, 351–364. [CrossRef]
4. Taylor, J.; Wilkinson, P.; Davies, M.; Armstrong, B.; Chalabi, Z.; Mavrogianni, A.; Symonds, P.; Oikonomou, E.; Bohnenstengel, S.I. Mapping the effects of urban heat island, housing, and age on excess heat-related mortality in London. *Urban Clim.* **2015**, *14*, 517–528. [CrossRef]
5. Wong, K.V.; Paddon, A.; Jimenez, A. Review of world urban heat islands: Many linked to increased mortality. *J. Energy Resour. Technol.* **2013**, *135*, 82–90. [CrossRef]
6. Li, J.; Niu, J.; Mak, C.M. Influences of variable thermal exposures on walking thermal comfort in hot summer-Physio-psychological responses. *Build. Environ.* **2023**, *239*, 110346. [CrossRef]
7. Chen, L.; Mak, C.M.; Hang, J.; Dai, Y.; Niu, J.; Tse, K.T. Large eddy simulation study on pedestrian-level wind environments around elevated walkways and influential factors in ideal urban street canyons. *Build. Environ.* **2023**, *235*, 110236. [CrossRef]
8. He, B.J.; Ding, L.; Prasad, D. Urban ventilation and its potential for local warming mitigation: A field experiment in an open low-rise gridiron precinct. *Sustain. Cities Soc.* **2020**, *55*, 102028. [CrossRef]
9. Liu, Y.; Xuan, C.; Xu, Y.; Fu, N.; Xiong, F.; Gan, L. Local climate effects of urban wind corridors in Beijing. *Urban Clim.* **2022**, *43*, 101181. [CrossRef]
10. Liu, X.; Huang, B.; Li, R.; Zhang, J.; Gou, Q.; Zhou, T.; Huang, Z. Wind environment assessment and planning of urban natural ventilation corridors using GIS: Shenzhen as a case study. *Urban Clim.* **2022**, *42*, 101091. [CrossRef]
11. Zhao, Y.; Xue, Y.; Mei, S.; Chao, Y.; Carmeliet, J. Enhancement of heat removal from street canyons due to buoyant approaching flow: Water tunnel PIV-LIF measurements. *Build. Environ.* **2022**, *226*, 109757. [CrossRef]
12. Xu, F.; Gao, Z.; Zhang, J.; Hu, Y.; Ding, W. Influence of typical street-side public building morphologies on the ventilation performance of streets and squares. *Build. Environ.* **2022**, *221*, 109331. [CrossRef]
13. Yang, H.; Chen, G.; Wang, D.; Hang, J.; Li, Q.; Wang, Q. Influences of street aspect ratios and realistic solar heating on convective heat transfer and ventilation in full-scale 2D street canyons. *Build. Environ.* **2021**, *204*, 108125. [CrossRef]
14. Kress, R. *Regionale Air Exchange Processes and Their Importance for the R Umliche Planning*; Institute of Environmental Protection of the University of Dortmund: Dortmund, Germany, 1979.
15. Givoni, B. *Climate Considerations in Building and Urban Design*; John Wiley & Sons: Hoboken, NJ, USA, 1998.
16. Brown, G.Z. *Sun, Wind, and Light. Architectural Design Strategies*; Wiley: Hoboken, NJ, USA, 1985.
17. VDI. *VDI-Guideline 3787, Part 1, Environmental Meteorology-Climate and Air Pollution Maps for Cities and Regions*; Beuth Verlag: Berlin, Germany, 1997.
18. Matzarakis, A.; Mayer, H. Mapping of urban air paths for planning in Munich. *Wiss. Ber. Inst. Meteor. Klimaforsch. Univ. Karlsr.* **1992**, *16*, 13–22.
19. Ren, C.; Yuan, C.; Ho, C.K.; Ng, Y.Y. A study of air path and its application in urban planning. *Urban Plan. Forum* **2014**, *3*, 52–60.
20. Yuan, C.; Ren, C.; Ng, E. GIS-based surface roughness evaluation in the urban planning system to improve the wind environment–A study in Wuhan, China. *Urban Clim.* **2014**, *10*, 585–593. [CrossRef]
21. Ling Chen, S.; Lu, J.; Yu, W.W. A quantitative method to detect the ventilation paths in a mountainous urban city for urban planning: A case study in Guizhou, China. *Indoor Built Environ.* **2017**, *26*, 422–437. [CrossRef]
22. Guo, F.; Zhang, H.; Fan, Y.; Zhu, P.; Wang, S.; Lu, X.; Jin, Y. Detection and evaluation of a ventilation path in a mountainous city for a sea breeze: The case of Dalian. *Build. Environ.* **2018**, *145*, 177–195. [CrossRef]
23. Lai, S.; Zhao, Y.; Fan, Y.; Ge, J. Characteristics of daytime land surface temperature in wind corridor: A case study of a hot summer and warm winter city. *J. Build. Eng.* **2021**, *44*, 103370. [CrossRef]
24. Mo, Z.; Liu, C.H.; Ho, Y.K. Roughness sublayer flows over real urban morphology: A wind tunnel study. *Build. Environ.* **2021**, *188*, 107463. [CrossRef]
25. Grimmond, C.; Sue, B.; Oke, T.R. Aerodynamic properties of urban areas derived from analysis of surface form. *J. Appl. Meteorol. Climatol.* **1999**, *38*, 1262–1292. [CrossRef]
26. Xu, F.; Gao, Z. Frontal area index: A review of calculation methods and application in the urban environment. *Build. Environ.* **2022**, *224*, 109588. [CrossRef]
27. Yang, J.; Wang, Y.; Xiao, X.; Jin, C.; Xia, J.C.; Li, X. Spatial differentiation of urban wind and thermal environment in different grid sizes. *Urban Clim.* **2019**, *28*, 100458. [CrossRef]

28. Wang, W.; Wang, D.; Chen, H.; Wang, B.; Chen, X. Identifying urban ventilation corridors through quantitative analysis of ventilation potential and wind characteristics. *Build. Environ.* **2022**, *214*, 108943. [CrossRef]
29. Wu, J.; Li, S.; Shen, N.; Zhao, Y.; Cui, H. Construction of cooling corridors with multiscenarios on urban scale: A case study of Shenzhen. *Sustainability* **2020**, *12*, 5903. [CrossRef]
30. Shi, Z.; Yang, J.; Zhang, Y.; Xiao, X.; Xia, J.C. Urban ventilation corridors and spatiotemporal divergence patterns of urban heat island intensity: A local climate zone perspective. *Environ. Sci. Pollut. Res.* **2022**, *29*, 74394–74406. [CrossRef]
31. Liu, D.; Zhou, S.; Wang, L.; Chi, Q.; Zhu, M.; Tang, W.; Zhao, X.; Xu, S.; Ye, S.; Lee, J.; et al. Research on the planning of an urban ventilation corridor based on the urban underlying surface taking Kaifeng city as an example. *Land* **2022**, *11*, 206. [CrossRef]
32. Tu, L.; Qin, Z.; Li, W.; Geng, J.; Yang, L.; Zhao, S.; Zhan, W.; Wang, F. Surface urban heat island effect and its relationship with urban expansion in Nanjing, China. *J. Appl. Remote Sens.* **2016**, *10*, 026037. [CrossRef]
33. Tao, Y.; Ye, R. Analysis of the spatio-temporal characteristics of Nanjing's urban expansion and its driving mechanisms. *ISPRS Int. J. Geo-Inf.* **2022**, *11*, 406. [CrossRef]
34. Chapman, S.; Watson, J.E.M.; Salazar, A.; Thatcher, M.; McAlpine, C.A. The impact of urbanization and climate change on urban temperatures: A systematic review. *Landscape Ecol.* **2017**, *32*, 1921–1935. [CrossRef]
35. Ng, E.; Cheng, V.; Chan, C. Urban Climatic Map and Standards for Wind Environment—Feasibility Study. Hong Kong Planning Department Final Report. 2012; 76p. Available online: https://www.researchgate.net/publication/283806656_Final_Report_of_Hong_Kong_Urban_Climatic_Map_and_Standards_for_Wind_Environment-_Feasibility_Study (accessed on 11 December 2023). [CrossRef]
36. Xie, P.; Yang, J.; Sun, W.; Xiao, X.; Xia, J.C. Urban scale ventilation analysis based on neighborhood normalized current model. *Sustain. Cities Soc.* **2022**, *80*, 103746. [CrossRef]
37. Xie, P.; Yang, J.; Wang, H.; Liu, Y.; Liu, Y. A New method of simulating urban ventilation corridors using circuit theory. *Sustain. Cities Soc.* **2020**, *59*, 102162. [CrossRef]
38. Wong, M.S.; Nichol, J.E.; To, P.H.; Wang, J. A simple method for designation of urban ventilation corridors and its application to urban heat island analysis. *Build. Environ.* **2010**, *45*, 1880–1889. [CrossRef]
39. Hsieh, C.M.; Huang, H.C. Mitigating urban heat islands: A method to identify potential wind corridor for cooling and ventilation. *Comput. Environ. Urban Syst.* **2016**, *57*, 130–143. [CrossRef]
40. Douglas, D.H. Least-cost path in gis using an accumulated cost surface and slopelines. *Cartogr. Int. J. Geogr. Inf. Geovis.* **1994**, *31*, 37–51. [CrossRef]
41. Peng, F.; Wong, M.S.; Wan, Y.; Nichol, J.E. Modeling of urban wind ventilation using high resolution airborne LiDAR data. *Comput. Environ. Urban Syst.* **2017**, *64*, 81–90. [CrossRef]
42. Roy, D.P.; Wulder, M.A.; Loveland, T.R.; Woodcock, C.E.; Allen, R.G.; Anderson, M.C.; Helder, D.; Irons, J.R.; Johnson, D.M.; Kennedy, R.; et al. Landsat-8: Science and product vision for terrestrial global change research. *Remote Sens. Environ.* **2014**, *145*, 154–172. [CrossRef]
43. Du, Y.; Zhang, Y.; Ling, F.; Wang, Q.; Li, W.; Li, X. Water bodies' mapping from Sentinel-2 imagery with modified normalized difference water index at 10-m spatial resolution produced by sharpening the SWIR band. *Remote Sens.* **2016**, *8*, 354. [CrossRef]
44. Qin, Z.; Karnieli, A.; Berliner, P. A mono-window algorithm for retrieving land surface temperature from Landsat TM data and its application to the Israel-Egypt border region. *Int. J. Remote Sens.* **2001**, *22*, 3719–3746. [CrossRef]
45. Likas, A.; Vlassis, N.; Verbeek, J.J. The global k-means clustering algorithm. *Pattern Recognit.* **2003**, *36*, 451–461. [CrossRef]
46. Xu, Y.; Wang, W.; Chen, B.; Chang, M.; Wang, X. Identification of ventilation corridors using backward trajectory simulations in Beijing. *Sustain. Cities Soc.* **2021**, *70*, 102889. [CrossRef]
47. Huang, J.; Wang, Y. Identification of ventilation corridors through a simulation scenario of forest canopy density in the metropolitan area. *Sustain. Cities Soc.* **2023**, *95*, 104595. [CrossRef]
48. Li, R.; Zeng, F.; Zhao, Y.; Wu, Y.; Niu, J.; Wang, L.L.; Gao, N.; Shi, X. CFD simulations of the tree effect on the outdoor microclimate by coupling the canopy energy balance model. *Build. Environ.* **2023**, *230*, 109995. [CrossRef]
49. Aboelata, A.; Sodoudi, S. Evaluating the effect of trees on UHI mitigation and reduction of energy usage in different built up areas in Cairo. *Build. Environ.* **2020**, *168*, 106490. [CrossRef]
50. Mohammadi, M.; Tien, P.W.; Calautit, J.K. Numerical evaluation of the use of vegetation as a shelterbelt for enhancing the wind and thermal comfort in peripheral and lateral-type skygardens in highrise buildings. *Build. Simul.* **2023**, *16*, 243–261. [CrossRef]
51. Guo, A.; Yue, W.; Yang, J.; Li, M.; Xie, P.; He, T.; Zhang, M.; Yu, H. Quantifying the impact of urban ventilation corridors on thermal environment in Chinese megacities. *Ecol. Indic.* **2023**, *156*, 111072. [CrossRef]
52. Niu, S.; Liu, X.; Wang, A.; Chen, L.; Zhou, X.; Shi, X.; Yang, L.; Jin, X. Research on the influence of outdoor trees on natural ventilation performance of an academic building. *Build. Simul.* **2023**, *16*, 927–946. [CrossRef]
53. Grunwald, L.; Schneider, A.K.; Schroeder, B.; Weber, S. Predicting urban cold-air paths using boosted regression trees. *Landsc. Urban Plan.* **2020**, *201*, 103843. [CrossRef]
54. Fang, Y.; Gu, K.; Qian, Z.; Sun, Z.; Wang, Y.; Wang, A. Performance evaluation on multi-scenario urban ventilation corridors based on least cost path. *J. Urban Manag.* **2021**, *10*, 3–15. [CrossRef]
55. Han, L.; Zhao, J.; Zhang, T.; Zhang, J. Urban ventilation corridors exacerbate air pollution in central urban areas: Evidence from a Chinese city. *Sustain. Cities Soc.* **2022**, *87*, 104129. [CrossRef]

56. Fu, J.; Wang, Y.; Zhou, D.; Cao, S.-J. Impact of Urban Park Design on Microclimate in Cold Regions using newly developped prediction method. *Sustain. Cities Soc.* **2022**, *80*, 103781. [CrossRef]
57. Lan, H.; Lau, K.K.L.; Shi, Y.; Ren, C. Improved urban heat island mitigation using bioclimatic redevelopment along an urban waterfront at Victoria Dockside, Hong Kong. *Sustain. Cities Soc.* **2021**, *74*, 103172. [CrossRef]
58. Wang, C.; Ren, Z.; Chang, X.; Wang, G.; Hong, X.; Dong, Y.; Guo, Y.; Zhang, P.; Ma, Z.; Wang, W. Understanding the cooling capacity and its potential drivers in urban forests at the single tree and cluster scales. *Sustain. Cities Soc.* **2023**, *93*, 104531. [CrossRef]
59. Wicht, M.; Wicht, A. LiDAR-based approach for urban ventilation corridors mapping. *IEEE J. Sel. Top. Appl. Earth Obs. Remote Sens.* **2018**, *11*, 2742–2751. [CrossRef]

Disclaimer/Publisher's Note: The statements, opinions and data contained in all publications are solely those of the individual author(s) and contributor(s) and not of MDPI and/or the editor(s). MDPI and/or the editor(s) disclaim responsibility for any injury to people or property resulting from any ideas, methods, instructions or products referred to in the content.